JOC Article

Ligand and Substrate Effects on the Mechanism of Rhodium-Catalyzed Hydrogenation of Enamides

Patrick J. Donoghue, Paul Helquist, and Olaf Wiest*

Department of Chemistry and Biochemistry, University of Notre Dame, Notre Dame, Indiana, 46556-5670

owiest@nd.edu

Received September 18, 2006

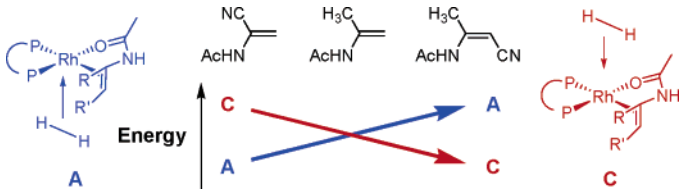

The rhodium-catalyzed hydrogenation reaction of enamides is studied computationally using the B3LYP/LACVP** level of theory for a range of ligands and substrates. Two model bidentate phosphine ligands, 1,2-bis(dimethylphosphino)ethane (DMPE) and (*Z*)-1,2-bis(dimethylphosphino) ethene (ZDMP), and two chiral bidentate phosphine ligands, (*R*,*R*)-MeDuPHOS and (*R*,*R*)-tetramethylbisoxaphospinane (TMBOP), are investigated in the hydrogenation of α-formamidoacrylonitrile as a model substrate. The ZDMP ligand is then studied for three additional substrates: *N*-(2-propenyl)formamide, (*Z*)-3-formamido-2-butenenitrile, and (*E*)-3-formamido-2-butenenitrile. The potential-energy surfaces calculated for the four ligands and α-formamidoacrylonitrile are in general agreement with previous computational studies using QM/MM (ONIOM) methods but show consistently higher relative barriers rather than lower. The calculated potential-energy surfaces of hydrogenations of various substrates with a common ligand indicate a mechanistic change based on substrate. The sequence of hydrogen transfer to the two olefinic carbons is calculated to change based on substrate electronics. This has a significant impact on the origins of enantioselectivity for such varied substrates as the first hydride transfer to the substrate is calculated to be irreversible for all substrates, independent of whether it occurs at the α or *β* carbon of the olefin.

Introduction

The synthesis of chiral amino acids is often performed through the asymmetric hydrogenation of enamides.[1] A representative example of this reaction is shown in Scheme 1. While the mechanism of the rhodium-catalyzed hydrogenation reaction has been well studied,[2] proper choice of chiral ligand for a new substrate is often left to trial and error. Experimental screening of ligands can be expensive and/or time-consuming. A computational method of screening ligands for a given reaction would greatly increase the efficiency of the process. In order to predict the optimal ligand for a given substrate, the origin of enantioselectivity in the reaction must be properly identified. The ligand would then be optimized by maximizing the energy difference between diastereomeric transition states of the

SCHEME 1. Rh-Catalyzed Hydrogenation of Enamides

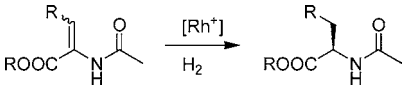

(1) (a) Noyori, R. *Angew. Chem., Int. Ed.* **2002**, *41*, 2008−2022. (b) Nagel, U.; Kinzel, E.; Andrade, J.; Prescher, G. *Chem. Ber.* **1986**, *119*, 3326. (c) Burk, M. J.; Feaster, J. E.; Nugent, W. A.; Harlow, R. L. *J. Am. Chem. Soc.* **1993**, *115*, 10125. (d) Liu, D.; Li, W.; Zhang, X. *Org. Lett.* **2002**, *4*, 4471. (e) Tang, W.; Zhang, X. *Angew. Chem., Int. Ed. Engl.* **2002**, *41*, 1612. (f) Xie, Y.; Lou, R.; Li, Z.; Mi, A.; Jiang, Y. *Tetrahedron: Asymmetry* **2000**, *11*, 1487. (g) Lou, R.; Mi, A.; Jiang, Y.; Qin, Y.; Li, Z.; Fu, F.; Chan, A. S. C. *Tetrahedron* **2000**, *56*, 5857. (h) Boaz, N. W.; Debenham, S. D.; Mackenzie, E. B.; Large, S. *E. Org. Lett.* **2002**, *4*, 2421. (i) Burk, M. J.; Allen, J. G.; Kiesman, W. F. *J. Am. Chem. Soc.* **1998**, *120*, 657. (j) Miyashita, A.; Takaya, H.; Souchi, T.; Noyori, R. *Tetrahedron* **1984**, *40*, 1245.

(2) (a) Halpern, J. *Science* **1982**, *217*, 401. (b) Chua, P. S.; Roberts, N. K.; Bosnich, B.; Okrasinski, S. J.; Halpern, J. *J. Chem. Soc., Chem. Commun.* **1981**, 1278. (c) Chan, A. S. C.; Pluth, J. J.; Halpern, J. *J. Am. Chem. Soc.* **1980**, *102*, 5952. (d) Landis, C. R.; Brauch, T. W. *Inorg. Chim. Acta* **1998**, *270*, 285. (e) Landis, C. R.; Halpern, J. *J. Am. Chem. Soc.* **1987**, *109*, 1746. (f) Schmidt, T.; Baumann, W.; Drexler, H.-J.; Arrieta, A.; Heller, D. *Organometallics* **2005**, *24*, 3842. (g) Brown, J. M.; Parker, D. *J. Org. Chem.* **1982**, *47*, 2722. (h) Brown, J. M.; Parker, D. *Organometallics* **1982**, *1*, 950. (i) Reetz, M. T.; Meiswinkel, A.; Mehler, G.; Angermund, K.; Graf, M.; Thiel, W.; Mynott, R.; Blackmond, D. G. *J. Am. Chem. Soc.* **2005**, *127*, 10305.

10.1021/jo0619276 CCC: $37.00
Published on Web 01/06/2007

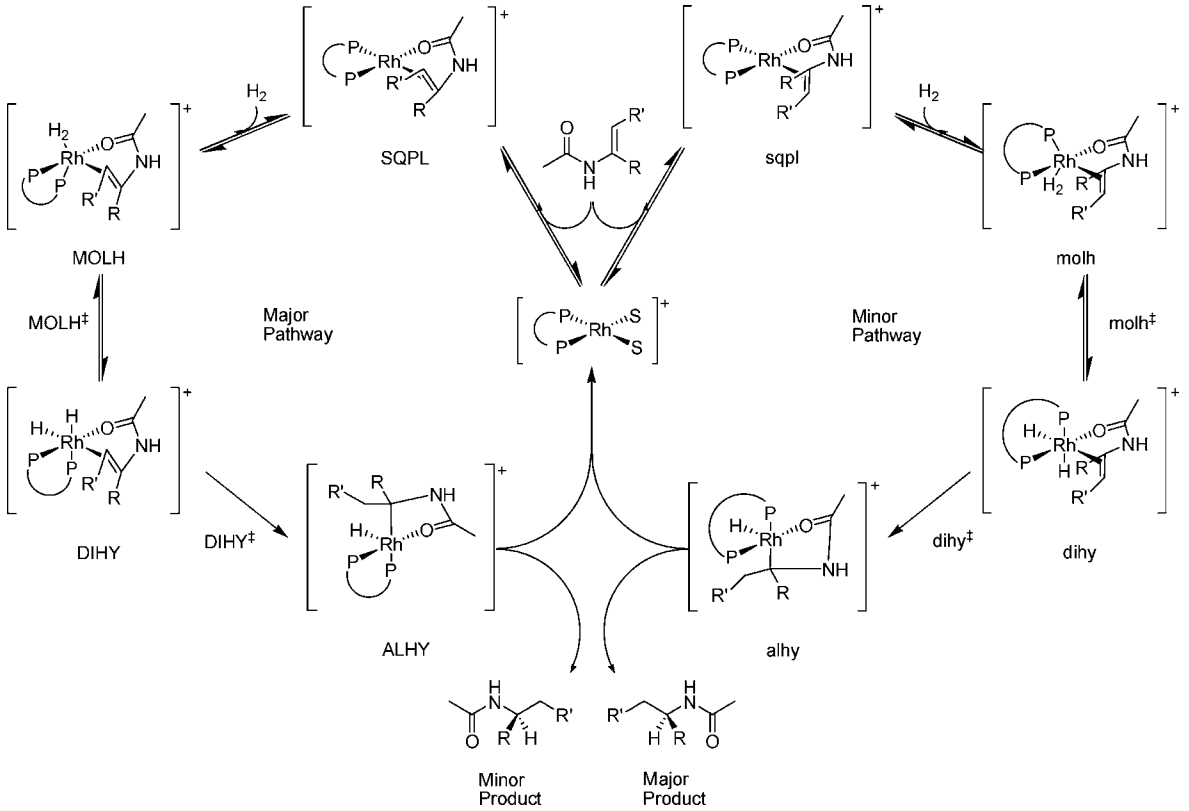

FIGURE 1. Overall mechanism of rhodium-catalyzed hydrogenation of enamides.

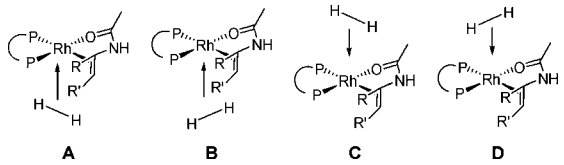

FIGURE 2. Mechanistic pathways derived from orientation of H_2 addition.

enantioselective step which leads to the enantiomeric products. A prerequisite for development of a model to properly predict enantioselectivity is that the mechanism of the reaction and especially the enantio-determining steps must be understood.

Mechanistic studies of this reaction have led to the development of the scheme shown in Figure 1.[2,3] With a chiral bisphosphine ligand the substrate first binds to the rhodium catalyst in one of two diastereomeric orientations to form a square planar complex, SQPL. Addition of H_2 proceeds through a trigonal bipyramidal molecular hydrogen complex, MOLH, followed by oxidative addition to form a dihydride species, DIHY. The first hydride transfer to the substrate forms an alkyl metal hydride species, ALHY. Whether this first hydride addition occurs to the α or β carbon of the alkene depends on the direction of the preceding H_2 addition. A second hydride transfer follows, generating the desired product and regenerating the catalyst after dissociation. Previous experimental studies have determined several important factors about the pathways. First, the overall reaction is irreversible. This was observed experimentally as there was no isotopic scrambling observed in unreacted substrate in the presence of D_2 and the rhodium catalyst.[2a,h] Computationally, both DFT[3a] and ONIOM[3b] studies have suggested that the barrier for the ALHY species reversing back to the DIHY species is about 25−30 kcal/mol on the energetically accessible mechanistic pathways, implying the first hydride transfer is irreversible. It is unclear whether the transition state of the oxidative addition of H_2, MOLH‡, or the hydride transfer, DIHY‡, is the rate-limiting step. The oxidative addition step has been suggested to be the first irreversible step in the catalytic cycle[2a,c,d] as the DIHY species could not be directly observed experimentally. Second, the enantioselectivity in the reaction is not determined by favorable complexation of the substrate to the catalyst. This "anti lock-and-key" motif, as it has been called previously,[2a,b,f] suggests that addition of H_2 to the system is the enantioselecting step. Only a single enantiomer can result from a given DIHY complex, and computational studies have demonstrated that isomerization between mechanistic pathways is energetically unfavorable.[3] While experimental observations have suggested that the rate-limiting step is also the enantio-determining step, the ability of the DIHY complex to lose H_2 has not been determined experimentally. Therefore, it would be inappropriate to model addition of H_2 to form the dihydride complex as the sole enantioselecting step without fully identifying the rate-limiting step.

There are four mechanistic pathways identified computationally by Landis and co-workers,[3] shown in Figure 2, which differ by the approach and orientation of the H_2 relative to the catalyst−substrate complex. Pathways A and B involve addition of H_2 syn to the β carbon in the alkene, while the C and D pathways have the addition syn to the α carbon. The first hydride transfer, forming the ALHY species, would involve addition of the hydride to the syn carbon. Pathways A and C are similar

(3) (a) Landis, C. R.; Hilfenhaus, P.; Feldgus, S. *J. Am. Chem. Soc.* **1999**, *121*, 8741. (b) Feldgus, S.; Landis, C. R. *J. Am. Chem. Soc.* **2000**, *122*, 12714. (c) Feldgus, S.; Landis, C. R. *Organometallics* **2001**, *20*, 2374.

in that the H_2 bond is parallel to the P−Rh−alkene bond, whereas the B and D pathways involve addition parallel to the P−Rh−O bond. These computational studies were done first as a full DFT study on a small model system utilizing PH_3 ligands[3a] and second as an ONIOM study utilizing the full DuPHOS ligand.[3b] Following Landis' nomenclature, two of the pathways, B and D, exhibit high barriers to oxidative addition of H_2 of about 20−25 kcal/mol in the DFT study and 30−35 kcal/mol in the ONIOM study. This barrier results from a large reorganization of the substrate binding to the rhodium catalyst. The C pathway was found to have a large barrier for the DIHY‡ transition structure, although the cause of this barrier is unknown. Addition of H_2 to the SQPL species along the C pathway is expected based on those data. As previously mentioned, experimental data[2a,c,d] suggest that addition of H_2 is irreversible. If this were the case, either the catalyst would be trapped as the DIHY-C complex or the C pathway would have to be catalytically productive, suggesting that the barrier might be a computational artifact. The remaining pathway, A, contains no large barriers and was proposed as the only catalytically active pathway.[3] There is a disparity between the two computational studies on the A pathway. The relative barrier heights for the oxidative addition and hydride transfer steps are reversed between the DFT and ONIOM studies. Whether or not this is an artifact of the computational method, namely, the fact that the ONIOM methods treats different parts of the molecule using different approaches, or the model system itself is undetermined. It may be possible that both barriers contribute to the rate-limiting step and the relative heights of the barriers are dependent on substrate and ligand substitutions. This further compounds the lack of experimental evidence available in separating these two key transition states to identify the source of enantioselectivity.

This paper will address several issues from the previous experimental and computational work in order to further elucidate the origin of enantioselectivity and mechanistic pathways leading to product formation. A full DFT evaluation of several ligands along the catalytically relevant steps will help identify which transition structure or structures are enantioselecting and determine which mechanistic pathways are available during the catalytic cycle. This will be achieved through comparison of the pathways utilizing several ligands, both chiral and achiral, as well as several substrates to analyze the effect of substrate electronics on the mechanism of the reaction. This is the first full DFT study of the reaction pathway for the various ligands and the first computational study over the reaction pathway for varied substrates.

Computational Details

All calculations were performed using Jaguar 5.5[4] with all structures fully optimized at the B3LYP level of theory using the LACVP** basis set. This basis set corresponds to a combination of the Los Alamos LANL2DZ ECP[5] for rhodium and the 6-31G** basis set for all other atoms. This basis set is similar to that used by Landis and co-workers in both the DFT and ONIOM computations previously.[3] All reported energies are enthalpies calculated at 298 K and 1 atm. Stationary points, both minima and transition structures, were confirmed through calculation of frequencies and identification of any negative eigenvalues. All energies given are in kcal/mol, and molecular distances are in angstroms, unless specified otherwise. Partial charges were calculated through electrostatic potential fitting.[6]

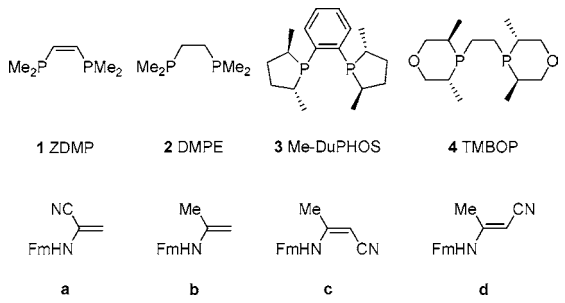

FIGURE 3. Ligands (**1**−**4**) and substrates (**a**−**d**) utilized in this study.

Results and Discussion

The nomenclature used herein is based on the mechanisms calculated previously.[3] The ligands studied are shown in Figure 3 and denoted by compound numbers **1**−**4**. The substrates used are also shown in Figure 3 and denoted by letters **a**−**d**. Ligand−substrate complexes in the mechanistic cycle are denoted by the appropriate compound numbers, followed by the intermediate abbreviation, as given in Figure 1, and the pathway name, as denoted in Figure 2. Due to the "anti lock-and-key" nature of the mechanism, the favorable diastereomeric complexation of the substrate to the catalyst leads to formation of the minor enantiomer in the reaction. Therefore, there are two manifolds based on the substrate complexation: major and minor. Intermediate and pathway names given in capitals denote the major manifold, which corresponds to favorable complexation of the substrate and catalyst that generates the minor product. The minor manifold, generating the major product, is denoted by lower case labels. For achiral ligands, only the capital labels will be utilized, as there is no differentiation between the two manifolds.

The previous DFT study of the reaction mechanism by Landis and co-workers[3a] utilized a model ligand system that would be impractical to approach experimentally. The present work studied the hydrogenation of the same model substrate used by Landis, formamidoacrylonitrile, but used larger model ligands, (*Z*)-1,2-bis(dimethylphosphino)ethene (ZDMP), **1**, and 1,2-bis-(dimethylphosphino)ethane (DMPE), **2**, as well as two C_2-symmetric chiral ligands, (*R*,*R*)-Me-DuPHOS, **3**, and (*R*,*R*)-tetramethylbisoxaphospinane (TMBOP), **4**. Only the two key transition structures, MOLH‡ and DIHY‡, are focused upon in this study. It is clear from previous experimental studies that the turnover limiting step occurs after addition of hydrogen[2a,c,d] and that formation of the ALHY species is irreversible.[2a,b,f] Any enantioselectivity in the reaction must therefore be derived during these key steps in the catalytic cycle. The calculated reaction pathway therefore includes these two transition structures, the surrounding minima, and the initial square planar catalyst−substrate complex, SQPL, as the energetic reference point.

The A and C pathways of substrate complex **1a** are shown in Figure 4. Since ligand **1** is achiral, there is only one possible SQPL complex and the pathways only differ by the approach

(4) *Jaguar 5.5*; Schrödinger, L.L.C.: Portland, OR, 1991−2003.
(5) Hay, P. J.; Wadt, W. R. *J. Chem. Phys.* **1985**, *82*, 299.
(6) (a) Chirlian, L. E.; Francl, M. M. *J. Comput. Chem.* **1987**, *8*, 894. (b) Woods, R. J.; Khalil, M.; Pell, W.; Moffat, S. H.; Smith, V. H., Jr. *J. Comput. Chem.* **1990**, *11*, 297. (c) Breneman, C. M.; Wiberg, K. B. *J. Comput. Chem.* **1990**, *11*, 361.

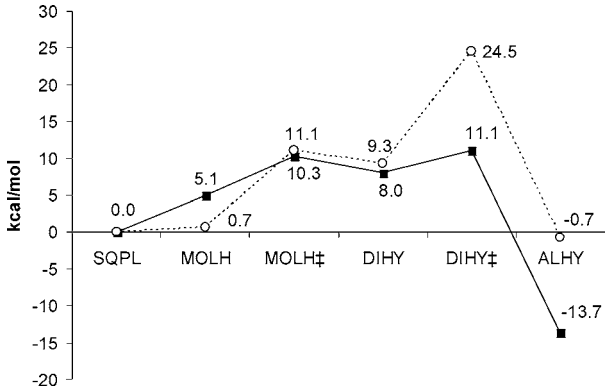

FIGURE 4. Calculated enthalpies for ligand complex **1a** over pathways A (■) and C (○).

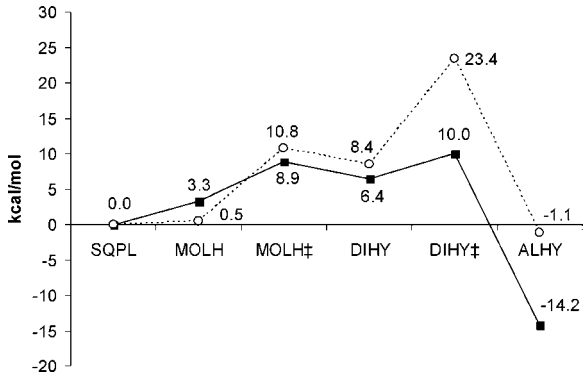

FIGURE 5. Calculated enthalpies for ligand complex **2a** over pathways A (■) and C (○).

of H_2. **1a**-MOLH-C is only 0.7 kcal/mol higher in energy than the **1a**-SQPL complex and is favored by 4.4 kcal/mol over **1a**-MOLH-A. The following transition structures, **1a**-MOLH‡-A and **1a**-MOLH‡-C, differ in energy by less than 1 kcal/mol at 10.3 and 11.1 kcal/mol, respectively. In the DIHY complex, **1a**-DIHY-A is favored over **1a**-DIHY-C, opposite of the preference for MOLH, by 1.3 kcal/mol. However, either energy difference is within the error limits that can be reasonably expected from the computational method. The barrier of formation of **1a**-DIHY‡-A from **1a**-DIHY-A is only 3.1 kcal/mol, but **1a**-DIHY‡-C is 13.2 kcal/mol higher in energy than **1a**-DIHY-C. The highest energy species on both pathways is at the DIHY‡ transition structure, being 11.1 kcal/mol on the A pathway and 24.5 kcal/mol on the C pathway. This large energy difference makes the C pathway very unlikely, in agreement with the results by Landis and co-workers.[3] After the DIHY‡ transition structure, the A and C pathways decrease in energy by 24.8 and 25.2 kcal/mol, respectively, to form the corresponding **1a**-ALHY complexes.

Figure 5 shows the reaction pathway for substrate complex **2a**. Similar to the case of ligand **1**, **2** is achiral and there is only one SQPL complex. **2a**-MOLH-C is only 0.5 kcal/mol higher in energy than **2a**-SQPL and favored over **2a**-MOLH-A by 2.8 kcal/mol. In analogy to **1**, **2a**-MOLH‡-A has a relative energy of 8.9 kcal/mol and is favored over **2a**-MOLH‡-C by 1.9 kcal/mol. There is a 2.0 kcal/mol energy difference between **2a**-DIHY-A and **2a**-DIHY-C. The relative energy along the A pathway then increases by 3.6 kcal/mol to form **2a**-DIHY‡-A with a relative energy of 10.0 kcal/mol. In comparison, the C pathway increases by 15.0 kcal/mol to 23.4 kcal/mol to form **2a**-DIHY‡-C. Once again, the DIHY‡ transition structure is the highest energy species on both pathways. The two pathways then decrease in energy 24.2 kcal/mol on the A pathway and 24.5 kcal/mol on the C pathway to form the corresponding **2a**-ALHY complexes.

The reaction profile of substrate complex **3a** is shown in Figure 6. Since the ligand Me-DuPHOS **3** is chiral, there are two reaction manifolds, with the SQPL complex and following reaction pathway proceeding to the left of center and the sqpl complex and following reaction pathway proceeding to the right of center. **3a**-sqpl is 2.8 kcal/mol higher in energy than **3a**-SQPL. On the C pathway, **3a**-MOLH-C is 1.7 kcal/mol higher in energy than **3a**-SQPL and **3a**-molh-c is 1.1 kcal/mol higher in energy than **3a**-sqpl-c. In analogy to **1a** and **2a**, **3a**-MOLH-A and **3a**-molh-a are higher in energy than the corresponding C pathway complexes. **3a**-MOLH-A and **3a**-molh-a have relative energies of 9.9 and 6.9 kcal/mol, respectively. On the minor manifold, **3a** follows a pattern similar to **1a** and **2a** in that **3a**-molh‡-c is now higher in energy than **3a**-molh‡-a, 14.0 and 12.4 kcal/mol, respectively. The major manifold does not follow this trend. **3a**-MOLH‡-C with a relative energy of 11.9 kcal/mol is 3.3 kcal/mol lower in energy than **3a**-MOLH‡-A. The pattern of the relative energies of the A and C pathways holds for the two manifolds at the DIHY intermediate as well. **3a**-DIHY-C is more stable than **3a**-DIHY-A with relative energies of 10.7 and 12.6 kcal/mol, respectively. **3a**-dihy-a is energetically favored over **3a**-dihy-c by 1.8 kcal/mol. **3a**-DIHY‡-A has a relative energy of 14.5 kcal/mol, 1.9 kcal/mol higher than **3a**-DIHY-A, and **3a**-dihy‡-a is at 12.2 kcal/mol, which is 1.2 kcal/mol higher in energy than **3a**-dihy-a. It can therefore be concluded that the barriers along pathway A are relatively low and that the minor reaction of the minor complex sqpl is favored. In comparison, the C pathway exhibits much larger barriers, analogous to **1a** and **2a**. **3a**-DIHY‡-C has a relative energy of 24.2 kcal/mol, 13.5 kcal/mol higher than **3a**-DIHY-C. Similarly, **3a**-dihy‡-c has a relative energy of 26.0 kcal/mol, 13.2 kcal/mol higher than **3a**-dihy-c. There is again a large energy release to form the alkyl hydride complexes on all manifolds and pathways. In all four reaction pathways shown in Figure 6 formation of the alkyl metal hydride species from the corresponding dihydride complex is calculated to be exothermic by more than 25 kcal/mol, making this step irreversible.

Figure 7 shows the energy profile of substrate complex **4a** derived from the TMBOP ligand **4**. The layout of the profile is analogous to that of **3a** in Figure 6. **4a**-sqpl is 3.5 kcal/mol higher in energy than **4a**-SQPL. The C pathway is again energetically favored over the A pathway at the MOLH intermediate on both manifolds. **4a**-MOLH-C is favored over **4a**-MOLH-A by 4.6 kcal/mol, while the energy difference between **4a**-molh-c and **4a**-molh-a in the minor manifold is only 0.7 kcal/mol. The pathways of **4a** mirror those of **3a** described previously. **4a**-MOLH‡-C, with a relative energy of 12.5 kcal/mol, is favored over **4a**-MOLH‡-A by 1.9 kcal/mol, and **4a**-molh‡-a is lower in energy than **4a**-molh‡-c with relative energies of 12.1 and 15.0 kcal/mol, respectively. Similarly, **4a**-DIHY-C is 0.5 kcal/mol lower in energy than **4a**-DIHY-A and **4a**-dihy-a is lower in energy than **4a**-dihy-c, with relative energies of 10.4 and 12.7 kcal/mol, respectively. The C pathways again have large energy barriers with **4a**-DIHY‡-C increasing from 11.6 to 23.7 kcal/mol and **4a**-dihy‡-c increasing from 12.7 to 25.6 kcal/mol. The A pathways do not have these large barriers with **4a**-DIHY‡-A increasing only 1.2 kcal/mol

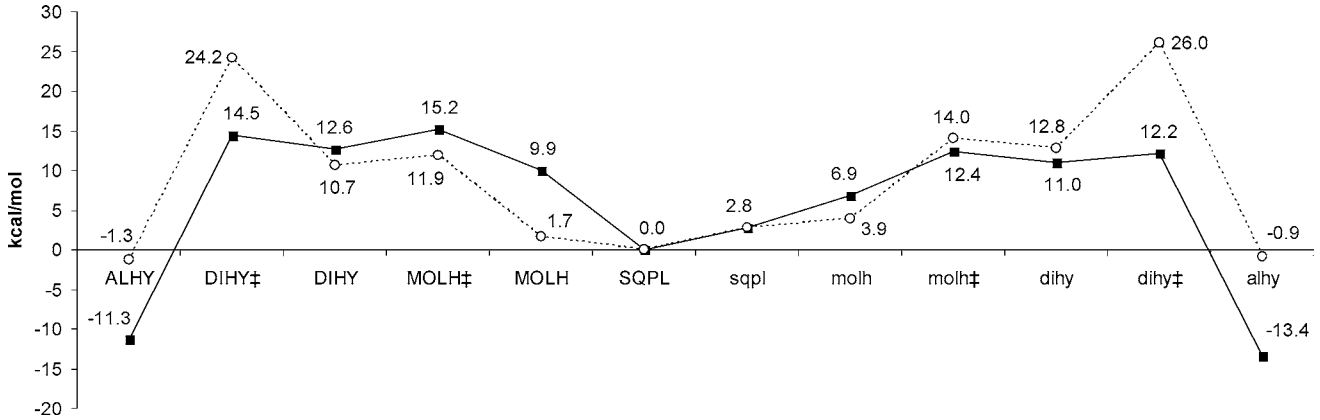

FIGURE 6. Calculated enthalpies for ligand complex **3a** over pathways A (■) and C (○).

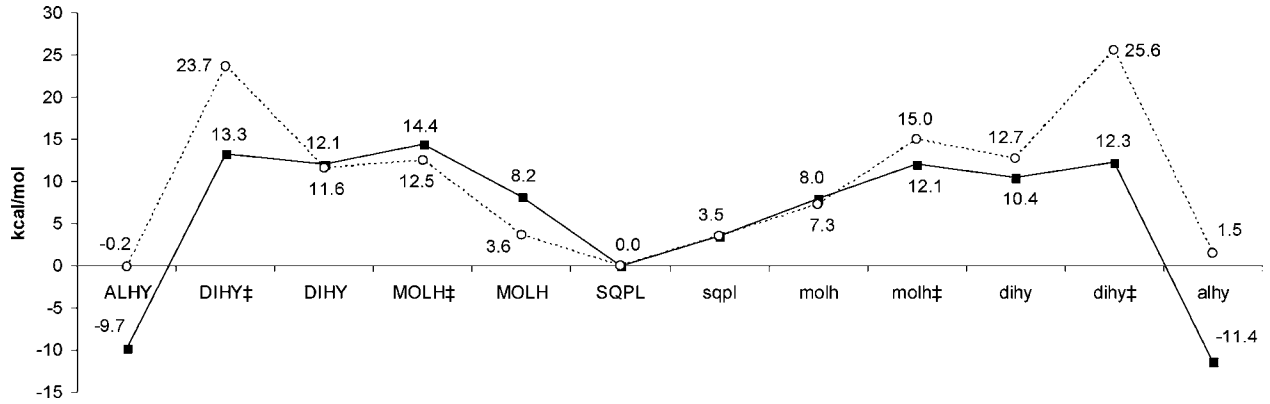

FIGURE 7. Calculated enthalpies for ligand complex **4a** over pathways A (■) and C (○).

and **4a**-dihy‡-a increasing only 1.9 kcal/mol. As was the case for **3a**, all of these transition structures resemble the reactants, as is expected for the highly exothermic formation of the alkyl hydride complexes in all cases. Remarkably, the energy difference from the transition structures to the corresponding alkyl hydride complexes is between 23 and 24 kcal/mol in all cases, even though the relative energies of the individual species in the four different pathways differ significantly. This indicates that the structural origin of the energy difference, namely, stabilization of the negative charge, is similar in the transition structures and the alkyl hydride complexes, as will be discussed later.

The Me-DuPHOS complex, **3a**, had been previously studied using a three-level ONIOM approach.[3a] The core region, defined as the substrate, the Rh atom, and an ethylene diphosphine ligand, was treated at the B3LYP/LANL2DZ level of theory. Adjacent alkyl groups were treated in the intermediate region with the smaller LANL2MB basis set, while the remaining atoms of the Me-DuPHOS ligand were treated at the UFF level. As discussed earlier, this led to inconsistencies between the results from the full DFT treatment of a model system and the results from the ONIOM calculations, but it is not clear if this is due to the level of theory or the structural changes. Therefore, the results of the ONIOM calculations were reinvestigated at the full DFT level. To confirm the large barriers on the B and D pathways obtained previously, single-point DFT energies at the ONIOM geometries were calculated and are compared to the ONIOM ΔE values in Table 1. The largest barriers on the B and D pathways agree within 2 kcal/mol and were still 10

TABLE 1. Comparison of DFT Energies at ONIOM Geometries to Previous ONIOM Calculations on the B and D Pathways[a]

	ONIOM	B3LYP//ONIOM
3a-SQPL-B	0.0	0.0
3a-SQPL-D	0.0	0.0
3a-sqpl-b	4.57	3.8
3a-sqpl-d	4.57	3.8
3a-IID‡-B	19.97	17.8
3a-IID‡-D	21.08	21.1
3a-iid‡-b	23.17	21.6
3a-iid‡-d	18.98	18.3
3a-MOLH-B	10.43	15.1
3a-MOLH-D	10.43	15.1
3a-molh-b	10.44	12.5
3a-molh-d	10.44	12.5
3a-MOLH‡-B	11.84	14.2
3a-MOLH‡-D	12.32	15.9
3a-molh‡-b	12.01	14.7
3a-molh‡-d	12.70	15.5
3a-DIHY-B	−6.07	−2.0
3a-DIHY-D	−3.22	1.7
3a-dihy-b	−5.21	−0.7
3a-dihy-d	−4.00	0.7
3a-DIHY‡-B	−4.69	−0.5
3a-DIHY‡-D	6.66	10.3
3a-dihy‡-b	−4.03	0.2
3a-dihy‡-d	6.20	9.6
3a-ALHY-B	−18.55	−15.9
3a-ALHY-D	−10.31	−9.3
3a-alhy-b	−17.25	−15.2
3a-alhy-d	−10.42	−9.5

[a] All energies in kcal/mol, and ONIOM data from ref 3b.

TABLE 2. Comparison of DFT Energies at ONIOM Geometries and DFT Geometries to Previous ONIOM Calculations on the A and C Pathways[a]

	Major Manifold			Minor Manifold		
	ONIOM	B3LYP//ONIOM	B3LYP	ONIOM	B3LYP//ONIOM	B3LYP
3a-SQPL-A	0.0	0.0	0.0	4.57	3.8	3.1
3a-SQPL-C	0.0	0.0	0.0	4.57	3.8	3.1
3a-MOLH-A	5.24	6.3	8.2	0.13	1.7	5.2
3a-MOLH-C	−3.09	−3.9	−0.1	1.26	−0.7	2.1
3a-MOLH‡-A	8.95	11.9	14.6	4.41	8.6	11.8
3a-MOLH‡-C	4.20	7.4	11.3	8.08	10.2	13.3
3a-DIHY-A	5.74	10.2	10.4	1.24	6.2	8.8
3a-DIHY-C	1.85	5.6	8.5	4.77	9.6	10.6
3a-DIHY‡-A	5.89	10.3	13.2	2.16	7.4	11.1
3a-DIHY‡-C	13.69	19.4	23.8	17.43	22.6	25.5
3a-ALHY-A	−22.37	*b*	−15.5	−24.79	−21.2	−17.6
3a-ALHY-C	−10.31	−9.32	−5.6	−10.42	−9.5	−5.3

[a] All energies in kcal/mol and ONIOM data from ref 3b. [b] Wavefunction did not converge at ONIOM geometry.

kcal/mol higher in energy than either diastereomeric manifold on the A pathway. Therefore, the B and D pathways are not considered to be relevant for catalysis, in agreement with the results of Landis and co-workers.[3] The A and C pathways were also calculated at the DFT level for the ONIOM geometries and then reoptimized at the DFT level. Comparison of these DFT results, single-point and reoptimized, to the ONIOM ΔE values are shown in Table 2 and shows general agreement between the two methods in relative but not absolute terms. The single-point DFT energies were generally higher than the corresponding ONIOM energies. The largest deviations between the two methods were at the two transition states, MOLH‡ and DIHY‡, and the DIHY intermediate, with energy differences ranging from 2.1 to 5.7 kcal/mol. The reoptimized DFT energies were even higher in relative energy, with the differences between the two transition states and DIHY intermediate ranging from 5.2 to 10.1 kcal/mol. Qualitatively, both the single-point and reoptimized geometries found large energetic barriers at DIHY‡-C from 19.1 to 25.0 kcal/mol, and the expected enantiomer is derived from the minor manifold of the A pathway, in excellent enantiomeric excess. Furthermore, the relative energies of the diastereomeric transition structures on the C pathway would favor formation of the *S* enantiomer, whereas (*R*,*R*)-Me-DuPHOS has been shown experimentally to generate the *R* enantiomer almost exclusively.[7]

Analysis of the results for the other three ligands, in **1a**, **2a**, and **4b**, shows agreement with the mechanistic pathways proposed previously[2,3] and with **3a** described above. All four ligands show common characteristics. First, the energy difference between MOLH‡-A and DIHY‡-A is very small. Specifically, the calculated relative energies between the two transition structures are 0.8 and 1.1 kcal/mol for the two model ligands, **1a** and **2a**, respectively. Complex **3a** is calculated to have the DIHY‡-A transition structure lower in energy on both the major and minor manifolds by 0.9 and 0.4 kcal/mol, respectively. **4a**-DIHY‡-A is lower in energy by 1.1 kcal/mol; however, **4a**-molh‡-a is calculated to be lower in energy by 0.2 kcal/mol. All of these energy differences are within the limits of accuracy of the computational method. Both previous computational studies calculated the energy difference to be on the order of 3 kcal/mol,[3a,b] although disagreeing on which transition structure was higher in energy. The previous DFT study suggested that the DIHY‡ transition structure was higher in energy than the MOLH‡ transition structure, while the ONIOM study showed the reverse. Second, all four ligands clearly favor the A pathway over the C pathway. The energy difference between DIHY‡-A and DIHY‡-C for all four ligands is quite large, ranging from 9 to 15 kcal/mol. The C pathway would therefore have a prohibitively high barrier at this step, thus favoring the A pathway almost exclusively. Similar to **3a**, the relative energies of the two manifolds on the C pathway of **4a** would also favor product formation from the major manifold. Experimentally, the hydrogenation has been shown to generate the *R* enantiomer, similar to **3**, which is derived from the minor manifold.[2a,b,f] Computational and experimental results therefore agree that the C pathway is not viable with substrate **a**.

To probe the origin of the large energetic difference between the two DIHY‡ transition structures, the six structures calculated for DIHY‡-C were compared to the corresponding DIHY‡-A structures. Representative structures of **1a**-DIHY‡-A and **1a**-DIHY‡-C are shown in Figure 8. From these structures, the differences in steric interactions between the A and C pathway are seen to be minimal. This is consistent with the previously calculated, small PH_3 model system, where no close steric contacts are expected on any pathway.[3a] The barrier is therefore most likely electronic in nature. The energy difference between the A and C pathways should therefore be sensitive to the electronic structure of the substrate, which can be manipulated by substitution. This was investigated by altering the substituents on the substrate from the electron-withdrawing cyano group on the carbon α to the amide, used to model the ester, to an electron-donating methyl group and subsequently adding a β-cyano group in both *Z* and *E* geometries to reverse the polarity of the alkene. Partial charges were calculated to fit the molecular electrostatic potential, and the results of these calculations for the α and β carbons of the olefin are shown in Figures 9−12 for **1a**, **1b**, **1c**, and **1d** respectively.

The partial charges for C_α are all calculated to be positive, and the charges for C_β are calculated to be negative with one exception. The largest difference in these polarizations for the A and C pathways for the four substrates occurs at the DIHY‡ transition structure. In general, the A pathway becomes less polarized and the C pathway becomes more polarized at this transition structure, although the relative amount changes based on substitution. For **1a** the A pathway changes by 0.17 e^- from

(7) (a) Burk, M. J.; Wang, Y. M.; Lee, J. R. *J. Am. Chem. Soc.* **1996**, *118*, 5142. (b) Burk, M. J.; Casy, G.; Johnson, N. B. *J. Org. Chem.* **1998**, *63*, 6084. (c) Gridnev, I. D.; Higashi, N.; Imamoto, T. *J. Am. Chem. Soc.* **2000**, *122*, 10486. (d) Gridnev, I. D.; Yasutake, M.; Higashi, N.; Imamoto, T. *J. Am. Chem. Soc.* **2001**, *123*, 5268.

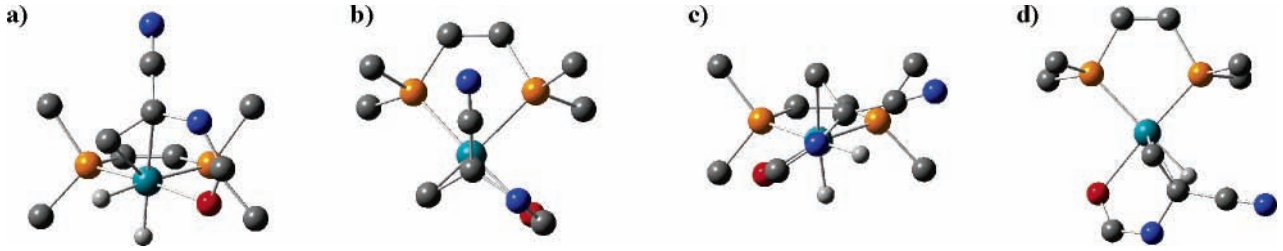

FIGURE 8. Calculated geometries of **1a**-DIHY‡-A (a) along and (b) above the rhodium−phosphine plane and **1a**-DIHY‡-C (c) along and (d) above the rhodium−phosphine plane.

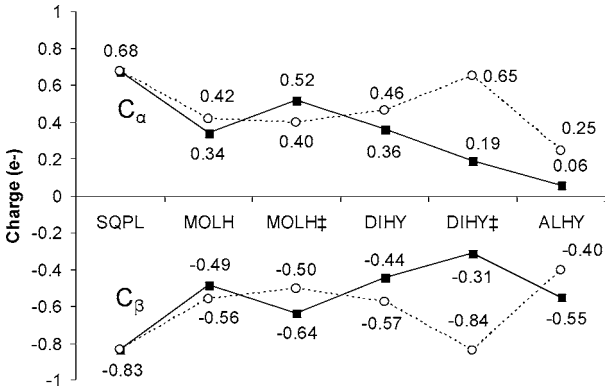

FIGURE 9. Calculated ESP charges for ligand complex **1a** over pathways A (■) and C (○).

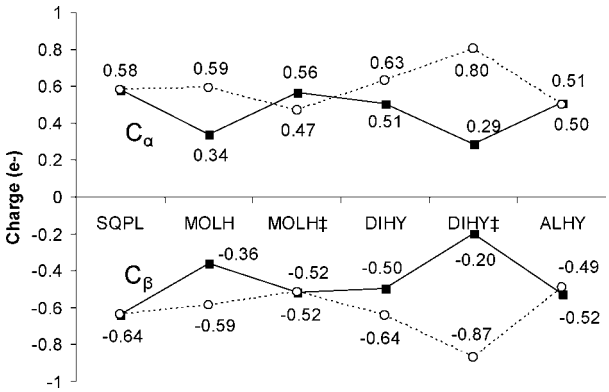

FIGURE 10. Calculated ESP charges for ligand complex **1b** over pathways A (■) and C (○).

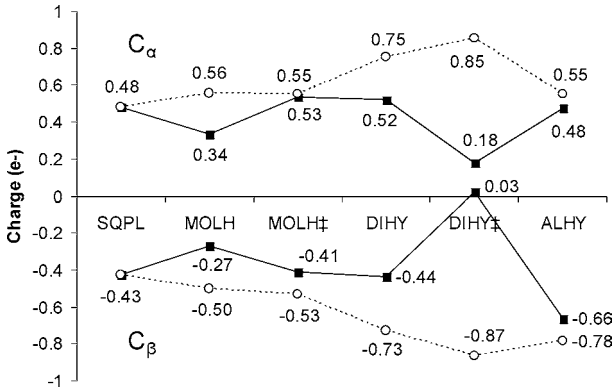

FIGURE 11. Calculated ESP charges for ligand complex **1c** over pathways A (■) and C (○).

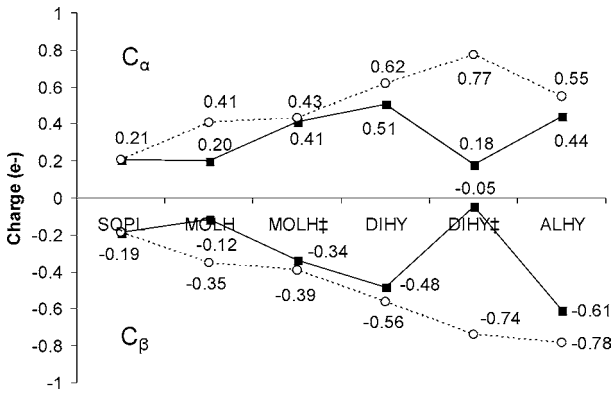

FIGURE 12. Calculated ESP charges for ligand complex **1d** over pathways A (■) and C (○).

DIHY to DIHY‡ on C_α and −0.13 e⁻ from DIHY to DIHY‡ on C_β. As the substitution pattern reverses polarity, the amount of change in partial charge between these points on the A pathway increases. Changing the cyano group to a methyl group in **1b** increases the changes to 0.22 and −0.30 e⁻ for C_α and C_β, respectively. Addition of the cyano group on the β carbon further increases this change. **1c** shows changes of 0.34 e⁻ on C_α and −0.47 e⁻ on C, and **1d** is calculated to have changes of 0.33 e⁻ on C and −0.43 e⁻ on C_β. A similar, but opposite, effect is observed on the C pathway as well. A larger change is observed for **1a**, −0.19 and 0.27 e⁻ for C_α and C_β, than for **1b**, −0.17 and 0.23 e⁻. The β-cyano derivatives show even smaller deviations. **1c** changes by −0.10 and 0.14 e⁻, and **1d** changes by −0.15 and 0.18 e⁻ for C_α and C_β. The A pathway results in an ALHY species that has a rhodium-stabilized carbanion at the α carbon, and the C pathway has this anion at the β carbon. In **1a** the α anion is stabilized by the amide and the cyano group but the β anion is primary and not stabilized by any substitution.

The partial charge analysis indicates that there is a larger electronic reorganization on the C pathway than on the A pathway. Replacement of the cyano group with the methyl group in **1b** should destabilize the buildup of charge on the A pathway, and the β-cyano group in **1c** and **1d** should then stabilize the anion at the β position.

This hypothesis is supported by the results of the calculations, specifically the geometries and partial charge data. The effect of these groups on the geometry of DIHY‡ is shown in Figure 13 for the A pathway and Figure 14 for the C pathway. The forming C−H bond at the transition structure clearly shows the effect of the substituents on the transition structure. The length of the C−H bond for **1a**-DIHY‡-A is 1.69 Å, shortens to 1.59 Å for **1b**-DIHY‡-A, and further shortens to 1.57 and 1.56 Å for **1c**-DIHY‡-A and **1d**-DIHY‡-A, respectively. A similar, but opposite, effect is seen on the C pathway. The forming C−H bond is 1.46 Å for **1a**-DIHY‡-C, 1.51 Å for **1b**-DIHY‡-C, and 1.59 and 1.61 Å for **1c**-DIHY‡-C and **1d**-DIHY‡-C, respectively. There-

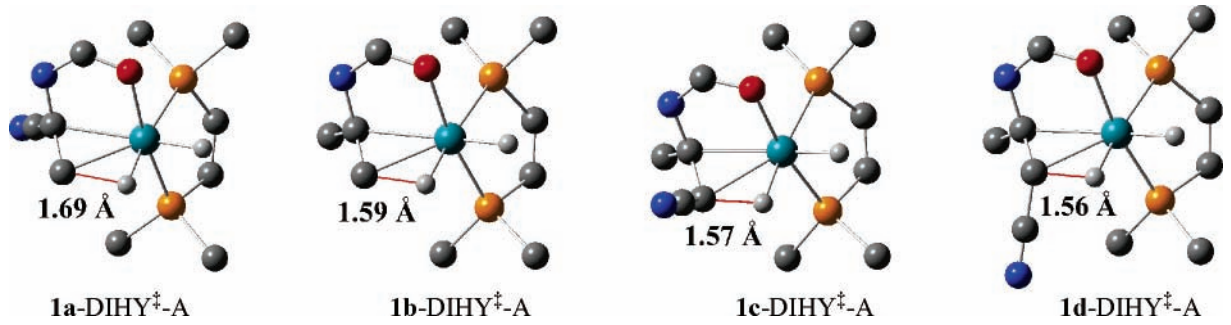

FIGURE 13. Calculated geometries of **1a**−**d**-DIHY‡-A with the forming C−H bond labeled.

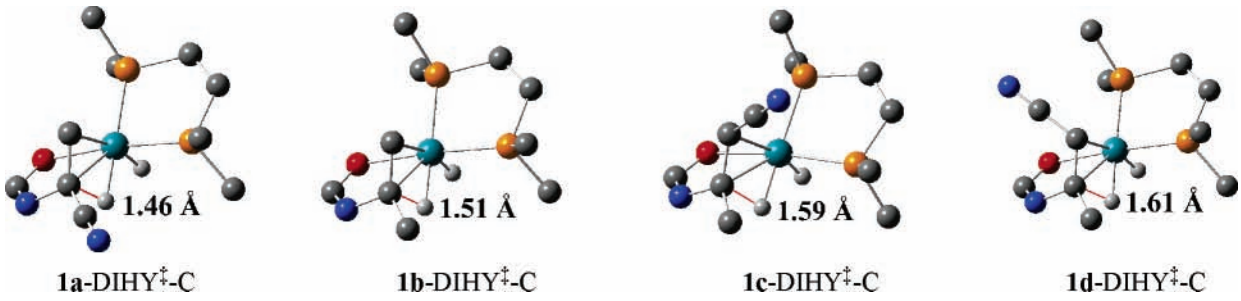

FIGURE 14. Calculated geometries of the DIHY‡-C species for **1a**−**d** with the forming C−H bond labeled.

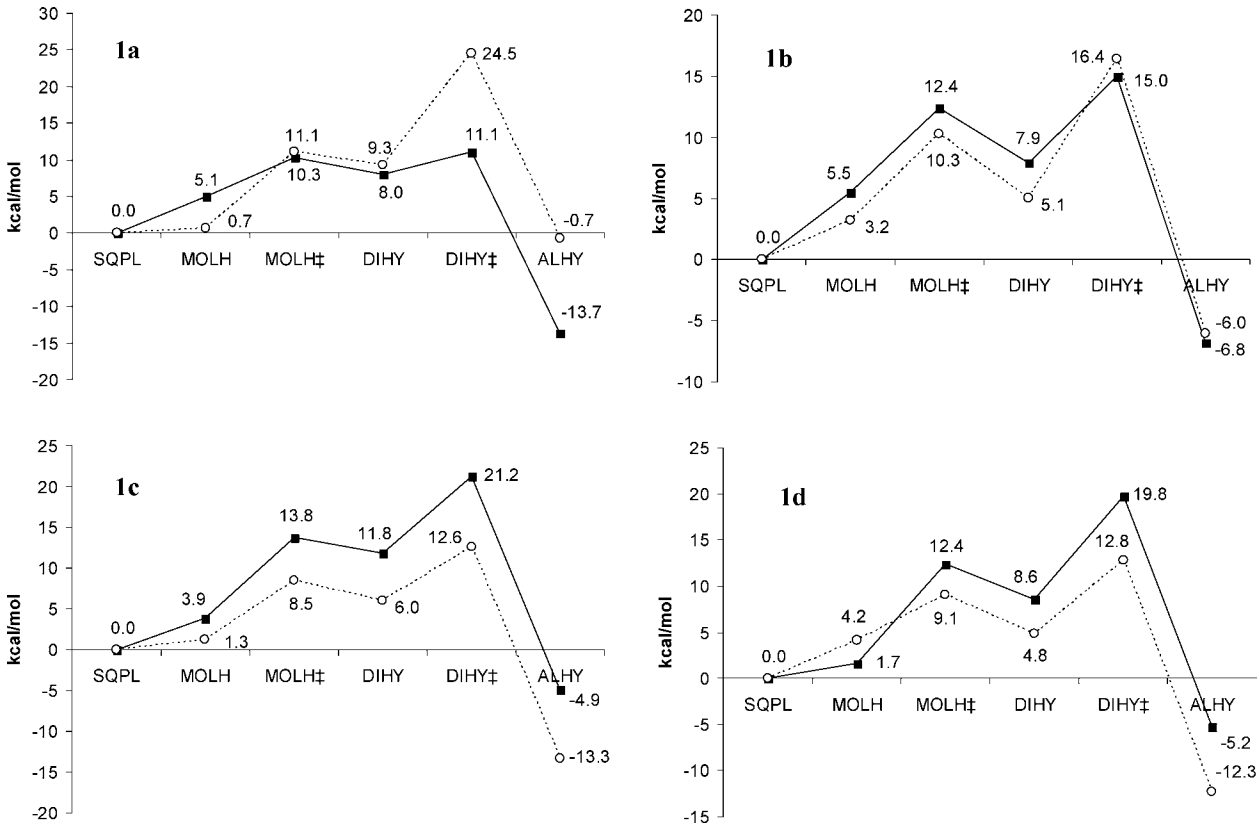

FIGURE 15. Comparison of the reaction enthalpies of substrates **1a**, **1b**, **1c**, and **1d** for pathways A (■) and C (○).

fore, removal of the electron-withdrawing group at the α position and reintroduction of the electron-withdrawing group at the β position simultaneously destabilizes the A pathway, as seen through the transition structure bond shortening, and stabilizes the C pathway, seen in the lengthening of the corresponding bond.

The complete energy profiles of the four substrates **a**−**d** in the reaction with ligand **1** are shown in Figure 15. As noted previously, the energy profile of the reaction for **1a** involves the A and C pathways being within 1 kcal/mol at MOLH‡ and DIHY. The two paths then differentiate at DIHY‡, where **1a**-DIHY‡-A is calculated to have a relative energy of 11.1 kcal/mol and **1a**-DIHY‡-C of 24.5 kcal/mol. Substrate **1b** shows a profound difference on the reaction profile. The C pathway is now lower in energy by 2.1 kcal/mol at MOLH‡ and 2.8 kcal/

mol at DIHY. The A pathway is still lower at energy at DIHY‡, but the energy difference has dropped from 13.4 kcal/mol in **1a** to 1.4 kcal/mol. In substrates **1c** and **1d** these changes are even stronger. The C pathway is now favored by 5.3 kcal/mol for substrate **1c** and 3.3 kcal/mol for substrate **1d** at MOLH‡ and favored by 5.8 kcal/mol for **1c** and 3.8 kcal/mol for **1d** at DIHY. At the DIHY‡ transition structure, the C pathway is now favored over the A pathway by 8.6 kcal/mol for **1c** and 7.0 kcal/mol for **1d**. The energy difference between MOLH‡ and DIHY‡ is also increased on the A pathway and decreased on the C pathway. For **1a** the differences are 0.8 kcal/mol for the A pathway and 13.4 kcal/mol on the C pathway. Substrate **1b** shows an increase on the A pathway to 2.6 kcal/mol and a decrease on the C pathway to 6.1 kcal/mol. The energy differences on the A pathway for **1c** and **1d** have increased further to 7.4 kcal/mol and on the C pathway decreased to 4.1 kcal/mol for **1c** and 3.7 kcal/mol for **1d**. The electronic effects of the substrate are most pronounced at DIHY‡, as is evident in the energy profiles and the charge analysis. The stabilization/destabilization of the two pathways is evident in the relative barrier heights of the A and C pathway at DIHY‡. For **1a** the C pathway has a prohibitively high energy at DIHY‡, whereas the two pathways are almost equivalent in energy for **1b**. The geometric isomers **1c** and **1d** show further destabilization of the A pathway and stabilization of the C pathway so that the A pathway now has a prohibitive barrier and only the C pathway should be catalytically active for such substrates. In qualitative terms, these differences can be attributed to electronically favorable, Michael-type hydride addition in the β-position relative to the electron-withdrawing nitrile group in **1a**-DIHY‡-A, **1c**-DIHY‡-C, and **1d**-DIHY‡-C. In contrast, the anti-Michael-sense hydride addition in **1a**-DIHY‡-C, **1c**-DIHY‡-A, and **1d**-DIHY‡-A is electronically unfavorable.

Conclusions

Rhodium-catalyzed hydrogenation reactions of enamides have been well-studied experimentally, and many chiral ligands have been utilized for asymmetric variants of the reaction. Mechanistic studies previously have focused on unsaturated α-amino acid derivatives, but the rhodium-catalyzed hydrogenation reaction has been used on substrates of significantly varied electronics. Substrates with alkyl or aryl α substituents or those with electron-withdrawing β substituents are also common in the literature.[1e,7,8] The present study suggests that the mechanism of hydrogenation may not be consistent for all substrates and is in agreement with a previous computational study as well.[3c] The mechanism appears to be fairly independent of ligand sterics but strongly depends on the electronics of the substrate, particularly the ability to stabilize the forming negative charge in DIHY‡ at either the α or the β carbon. On the A pathway the ALHY intermediate contains a Rh-stabilized carbanion on the α carbon, whereas the ALHY intermediate on the C pathway has a stabilized carbanion on the β carbon. The preference of A vs C pathway appears to be based on the ability of the substrate to stabilize the carbanion in addition to the stability offered by the Rh catalyst. For all substrates the amide substituent would stabilize carbanion formation at the α carbon, which would cause a bias toward the A pathway. Substrate **a**, being unsubstituted at the β carbon, offers no additional stability on the C pathway, and the nitrile group at the α carbon promotes hydride addition in a Michael fashion at the β carbon. Therefore, all substituents on substrate **a** are favorable toward the A pathway and unfavorable for the C pathway. Substrates **c** and **d** contain a nitrile moiety at the β carbon, thus promoting Michael addition at the α carbon. Electronically, the methyl group at the α carbon in substrates **b**, **c**, and **d** slightly destabilizes the carbanion at the α carbon. Substrate **b** has counteracting electronics between the methyl and amide, effectively canceling out and the two pathways are energetically similar. Addition of the Michael addition bias in **c** and **d** helps to promote the C pathway over the A pathway. Low-temperature NMR studies have previously identified the ALHY intermediate, and this intermediate would obviously be different for the A and C pathways due to the change in order of hydride addition. The calculated mechanistic switch should therefore be evident in a similar NMR study with substrates similar to **b**, **c**, or **d**.

The previous computational study using substrate complex **3a** in ONIOM appears to overestimate the relative energies of the system. The enthalpies of the DFT optimizations and the single-point energies at the ONIOM geometries both showed lower relative energies than the ONIOM geometries, although not by a consistent amount. The largest energy deviation between the ONIOM and DFT optimizations was at **3a**-MOLH-C, where the two methods disagreed by 8.6 kcal/mol, while at several points the two methods agreed within 1 kcal/mol. The calculated geometries between the two methods are similar, and there are no significant geometrical deviations. The reaction profile is also consistent between ONIOM and DFT optimizations. On the basis of the maximum energies of single transition structure geometries in the two manifolds, the DFT energies would predict an essentially identical enantiomeric excess of the reaction. The higher ONIOM energies would only affect the overall rate of the reaction, not the selectivity of the reaction.

The rate-limiting step in the reaction is subject to the substrate electronics. The energy profiles of complexes **1b**−**d** suggest that DIHY‡ is the rate-limiting step for both A and C pathways. The profiles of **1**−**4a** do not show any bias for either MOLH‡ or DIHY‡ as the rate-limiting step on the A pathway, and the C pathway is calculated to be energetically unfavorable and therefore catalytically inactive. On the basis of this information, any prediction of enantioselectivity for unsaturated α-amino acid derivatives, such as substrate **a**, should be based on a combination of the MOLH‡ and DIHY‡ transition states on the A pathway. Enantioselectivity predictions for substrates with varied electronics would have to account for both the A and C pathway, as in substrate **b**, or only the C pathway, as in substrates **c** and **d**. Development of a model for the enantioselectivity in the reaction, and its application in screening chiral ligands for the reaction would need to account for such substrate electronics and the corresponding available mechanistic pathways and transition structures.

Acknowledgment. We gratefully acknowledge the allocation of computer resources by the Center for Research Computing at the University of Notre Dame. P.J.D. is the recipient of a Schmitt Fellowship by the University of Notre Dame.

Supporting Information Available: Cartesian coordinates, imaginary frequencies, SCF energies, and enthalpies of all reactants and transition structures calculated. This material is available free of charge via the Internet at http://pubs.acs.org.

JO0619276

(8) (a) Li, W.; Waldkirch, J. P.; Zhang, X. *J. Org. Chem.* **2002**, 7618. (b) Zhou, Y.-G.; Tang, W.; Wang, W.-B.; Li, W.; Zhang, X. *J. Am. Chem. Soc.* **2002**, *124*, 4952. (c) Lee, S.-G.; Zhang, Y. J. *Org. Lett.* **2002**, *4*, 2429.